Intraglobular structures in multiblock copolymer chains from a Monte Carlo simulation

K. Lewandowski and M. Banaszak*

Faculty of Physics, A. Mickiewicz University ul. Umultowska 85, PL-61-614 Poznan, Poland

(Received 22 March 2011; revised manuscript received 15 June 2011; published 22 July 2011)

Multiblock copolymer chains in implicit nonselective solvents are studied by using a Monte Carlo method, which employs a parallel tempering algorithm. Chains consisting of 120 A and 120 B monomers, arranged in three distinct microarchitectures: $(10\text{-}10)_{12}$, $(6\text{-}6)_{20}$, and $(3\text{-}3)_{40}$, collapse to globular states upon cooling, as expected. By varying both the reduced temperature T^* and the compatibility between monomers ω, numerous intraglobular structures are obtained: diclusters (handshake, spiral, torus with a core, etc.), triclusters, and n clusters with $n > 3$ (lamellar and other), which are reminiscent of the block copolymer nanophases for spherically confined geometries. Phase diagrams for various chains in the (T^*,ω) space are mapped. The structure factor $S(k)$, for a selected microarchitecture and ω, is calculated. Since $S(k)$ can be measured in scattering experiments, it can be used to relate simulation results to an experiment. Self-assembly in those systems is interpreted in terms of competition between minimization of the interfacial area separating different types of monomers and minimization of contacts between chain and solvent. Finally, the relevance of this model to the protein folding is addressed.

DOI: 10.1103/PhysRevE.84.011806 PACS number(s): 82.35.Jk

I. INTRODUCTION

A single multiblock copolymer chain in a nonselective solvent is an interesting system to study because of its potential to form various nanostructures in a globular state, such as double droplet, lamellar, hand shake, spiral, and disordered globule [1]. Those nanostructures are reminiscent of phases observed in block copolymer melts [2,3], in general, and in confined geometries [4–9], in particular. Confinement can be one dimensional (thin films) [4], two dimensional (cylindrical pores) [5–7], and three dimensional (spherical pores) [8,9]. The latter is the most relevant analog for a single polymer chain in a poor solvent, since the chain collapses and tends to form a spherical globule. Copolymer chains in spherical confinement, with interaction parameters similar to those considered in this paper, were studied, using a coarse-grained model, in Ref. [8]. The following structures, corresponding to those identified in multiblock copolymer chains, were identified [8]: spheres with layers, helical-like or handshakelike structures, and tricluster structures.

Ordering of copolymer nanostructures is driven by both lowering the temperature, which results in decreasing the solvent quality, and lowering the compatibility between A and B, which leads to a coil-to-globule transition and a subsequent segregation of A and B monomers within the globule. There are interesting analogies:

(1) The formation of a globule is a condensation of monomers, which is similar to a gas-liquid transition,

(2) segregation of A and B monomers resembles disorder-order and order-order transitions, resulting in structures similar to those of copolymers in confined geometries.

At considerably lower temperatures, the polymer chains crystallize, undergoing both liquid-solid and solid-solid transitions, with interesting packing effects, as shown recently for homopolymers [10–12].

An additional motivation for this paper is its possible relation to structural transformations in biopolymers [13]. For example, the simplest models of proteins also employ only two types of building blocks that are hydrophilic, also referred to as polar (P) and hydrophobic (H) [14,15]. These models, despite their excessive simplicity, provide basic insight into the formation of secondary and tertiary structures, but in comparison to models with more types of monomers, they result in less cooperative folding and also in less designing sequences [13,16–18]. The sequence is referred to as designing when it can fold to the unique native state, that is, the ground state with the lowest energy.

The majority of sequences in the HP model lead to degenerate native states, unlike most proteins that exhibit the native state with fluctuations, which probe various conformational substates. Those substates are often very close to the native state and are caused by thermal fluctuations of atoms and slight displacements of amino acids [19]. Increasing the number of types of monomers with various interaction energies (for example, as calculated in Ref. [20]) can improve these models in terms of reproducing the properties of the real protein systems [21]. A modification of the HP model, such as a change in the interaction energy between H and P monomers, can also improve this model noticeably [18]. In this paper, we also use only two types of monomers, A and B, but in a nonselective solvent, and this can provide some insight into the ordering of proteins with H amino acids within the H core. It is worthwhile to reiterate that both monomers mimic the H behavior, at low temperatures, since the solvent is nonselective.

The specific goals of the paper are as follows:

(1) to identify intraglobular structures of long multiblock copolymer chains with different compatibilities,

(2) to construct phase diagrams for those structures,

(3) to calculate structure factors for selected chains,

(4) to relate results to the protein folding problem.

*Corresponding author: mbanasz@amu.edu.pl [http://www.simgroup.amu.edu.pl].

II. MODEL

A. Simulation box and environment

Simulation is performed in a cubic box, and the usual periodic boundary conditions are imposed. The simulation box size is sufficiently large for a chain to fit in and not to interact with itself across boundary conditions. We simulate a single polymer chain, and polymer-solvent interactions are included in an implicit manner in the polymer-polymer interaction potential [22]. This can be considered as a dilute polymer solution.

B. Polymer model

We use a coarse-grained model for the polymer chain with monomers of diameter σ also taken as the length unit. In this paper, by monomer, we mean the basic building unit of the coarse-grained chain. Monomers are of two types: A and B. Neighboring monomers along the chain are connected via the bond potential:

$$U_B(r) = \begin{cases} \infty & \text{for} \quad r < \sigma, \\ 0 & \text{for} \quad \sigma \leqslant r \leqslant \sigma + \eta, \\ \infty & \text{for} \quad r > \sigma + \eta, \end{cases} \tag{1}$$

where $\sigma + \eta$ is the maximum bond length and $\sigma + \frac{1}{2}\eta$ is considered to be the average bond length.

Monomers that are not adjacent along the chain (nonbonded monomers) interact via the following square well potential:

$$U_N(r) = \begin{cases} \infty & \text{for} \quad r < \sigma, \\ \epsilon_{ij} & \text{for} \quad \sigma \leqslant r \leqslant \sigma + \mu, \\ 0 & \text{for} \quad r > \sigma + \mu, \end{cases} \tag{2}$$

where $\sigma + \mu$ is the range of the interaction potential and ϵ_{ij} is the interaction energy between monomers of types i and j. We assume that $\mu = \frac{1}{4}\sigma$ and $\eta = \frac{1}{4}\sigma$ [23].

Chain bonds are not allowed to be broken, however, they are allowed to be stretched. Interaction parameter ϵ_{ij} is defined as

$$\begin{aligned} \epsilon_{AA} &= \epsilon_{BB} = -\epsilon, \\ \epsilon_{AB} &\in [-\epsilon; -0.1\epsilon]. \end{aligned} \tag{3}$$

The ϵ parameter, which is positive, serves as an energy unit to define the reduced energy per monomer E^*/N and the reduced temperature T^* as

$$\begin{aligned} E^*/N &= \left(\frac{E}{\epsilon}\right) \Big/ N, \\ T^* &= k_B T/\epsilon, \end{aligned} \tag{4}$$

where N is the number of chain monomers and k_B is the Boltzmann constant. Negative ϵ_{ij}'s indicate that there is an attraction between monomers, and the presence of the solvent is taken into account in an implicit manner [22]. By controlling the relative strength of this attraction, via T^*, we effectively vary solvent quality, from good to bad, which causes a collapse of the polymer chain from a swollen state to a globular state [23–25]. The swollen and collapsed states are separated by the Θ solvent state, where the chain is Gaussian. This state is characterized by a temperature T^*_Θ, which is on the order of unity $T^*_\Theta \sim 1$ for this model. Since we are interested in intraglobular structures, we mostly concentrate on temperatures below the Θ temperature.

Because we vary ϵ_{AB}'s in this paper, a dimensionless parameter $\omega = -\epsilon_{AB}/\epsilon$ is introduced, which is a measure of compatibility between A and B monomers. Lower values of ω mean lower compatibility. As we increase ω from 0.1 to 1, we make the monomers increasingly compatible, and for $\omega = 1$, they become identical, converting the copolymer chain into the homopolymer chain.

C. Polymer architecture

While we use only one chain length $N = 240$ with 120 A monomers and 120 B monomers, different multiblock microarchitectures are considered: $(10\text{-}10)_{12}$, $(6\text{-}6)_{20}$, and $(3\text{-}3)_{40}$. For the largest block size $(10\text{-}10)_{12}$, the A and B monomers are expected to separate more easily at low temperatures, but for smaller block sizes, it may be more difficult to separate them into two phases because of geometric frustrations.

D. Cluster count distribution

We differentiate between intraglobular structures by the number of clusters of A and B monomers and by the shape of those clusters. We define cluster as a group of monomers of the same type that are connected with each other either directly or via a connected path of monomers, and two monomers are connected if their distance is smaller than the range of the interaction potential. We count the clusters in simulation and determine the equilibrium cluster count distribution (CCD), which is the probability distribution for different counts of clusters.

For each chain architecture and ω, the CCD is calculated and is plotted as a function of T^*. These plots are used to determine the phase diagrams in the (T^*,ω) space for each microarchitecture. Since n clusters with different n can coexist for a given (T^*,ω), we show only the most probable structures in phase diagrams.

III. METHOD

We use the Metropolis [26] acceptance criteria for the Monte Carlo (MC) moves. The MC moves are chain rotations, translations, crankshaft rotations, and slithering snake moves. A MC step (MCS) is defined as an attempt to move each monomer of the chain once.

Moreover, we use parallel tempering (PT) (replica exchange) MC [27] with a feedback-optimized PT (FOPT) method [28,29]. In the PT method, M replicas of the system are simulated in parallel, each at a different temperature T^*_i, with i ranging from 1 to M. After a number of MCSs (in this paper, it is 100 MCSs), we try to exchange replicas with a neighboring T^*_i in random order with the probability,

$$p(T^*_i \leftrightarrow T^*_{i+1}) = \min\{1, \exp[-(\beta_i - \beta_{i+1})(U_{i+1} - U_i)]\}, \tag{5}$$

where $\beta_i = 1/k_B T^*_i$ and U_i is the potential energy of the replica at T^*_i.

A correctly adjusted PT method allows a better probing of the phase space of the system and prevents trapping in energy minima at low temperatures. Thus, it allows us to obtain better statistics in simulation, and after a single simulation, we

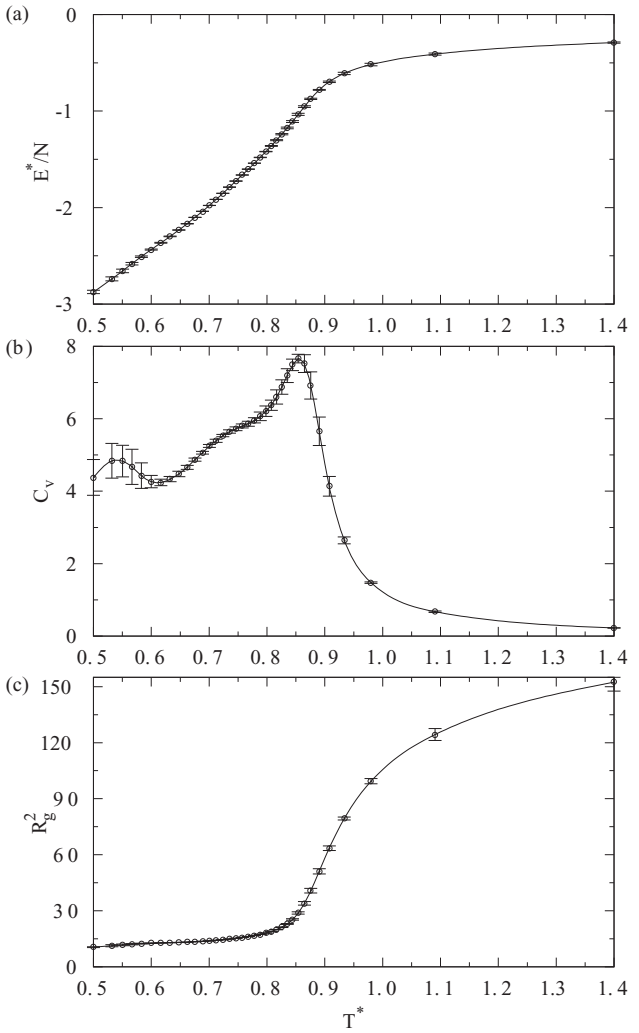

FIG. 1. Results for the $(10\text{-}10)_{12}$ chain (error bars are also shown): (a) reduced energy per monomer E^*/N as a function of reduced temperature T^*, (b) specific heat C_v as a function of T^*, (c) squared radius of gyration R_g^2 as a function of T^*.

obtain results for the selected range of temperatures. We use $M = 24$, 32, and 40 replicas.

A considerable challenge for the PT method is the selection of temperatures. As we are interested in globular states, thus, we mostly choose low temperatures $T^* < T^*_\Theta$. For chains $(3\text{-}3)_{40}$ and $(6\text{-}6)_{20}$, we used $T_i^* \in [0.3; 1]$. For the $(10\text{-}10)_{12}$ chain, we used $T_i^* \in [0.5; 1]$ because below 0.5, nothing seems to change in the polymer structure. However, in each case for $\epsilon_{AB} \approx -\epsilon$, the highest value of T^* was 1.1 because coil-to-globule transition occurred for $T^* > 1$. The FOPT method is used to obtain an optimized temperature set. In this method, we start with some temperature set (for example, linear or geometric) and run the simulation. In the next iteration, we obtain a more optimal temperature set. A few iterations are required to obtain the optimized temperature set. This method was described in detail in Ref. [28], and it was applied to a polymer system in Ref. [29] and in Ref. [30].

For each chain architecture, we run five iterations of FOPT, and we use the obtained temperature set in simulations. Each iteration of FOPT and each simulation consist of 5×10^5 MCSs in athermal conditions (mixing) and at least 4×10^7 MCSs in thermal conditions. The first 2×10^7 MCSs are used to equilibrate the system, and the rest is used to collect data.

IV. RESULTS AND DISCUSSION

A. Chain with $(10\text{-}10)_{12}$ microarchitecture

First, we present the results for the $(10\text{-}10)_{12}$ multiblock chain with a compatibility parameter $\omega = 0.1$. At high temperatures, this chain is in a coiled state, and it is expected to undergo the coil-to-globule transition upon cooling. Moreover, due to a low compatibility between A and B monomers, some ordered A- and B-rich nanostructures are also expected at low temperatures.

Indeed, the temperature dependencies for energy E^*/N, heat capacity C_v, and radius of gyration R_g^2 (in σ^2 units), shown in Fig. 1, indicate the above orderings as T^* is decreased. In particular, while E^*/N does not change much from high T^*'s to about $T^* \approx 1$, for smaller T^*'s, it decreases rapidly, and this corresponds to a maximum in C_v, observed in Fig. 1(b). Also, R_g^2 exhibits the most rapid change in this temperature region. Judging from the above and the position of the higher peak in C_v, we estimate the coil-to-globule transition temperature as approximately $T^*_{CG} \approx 0.85$. We observe that, below T^*_{CG}, R_g^2 is almost constant, decreasing slightly upon cooling. In Fig. 1(c), we can also observe a C_v maximum at about $T^* \approx 0.56$ and a bump in C_v at about $T^* \approx 0.75$. This is elucidated below in terms of the cluster formation.

Representative snapshots of the $(10\text{-}10)_{12}$ multiblock chain are shown in Fig. 2. A variety of globular structures can be seen, with the number of clusters decreasing upon cooling.

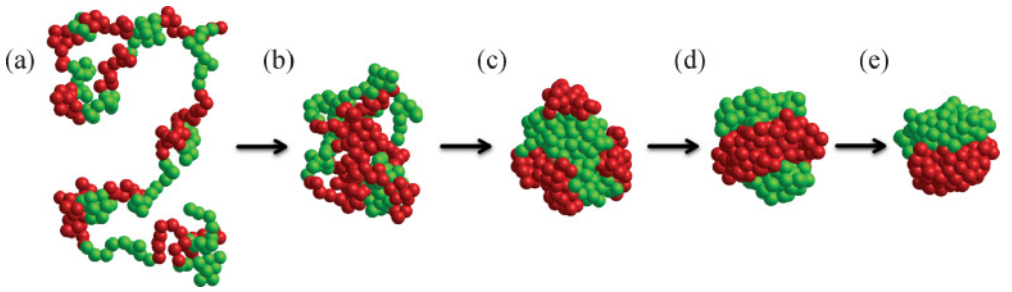

FIG. 2. (Color online) Representative snapshots of the $(10\text{-}10)_{12}$ chain with compatibility $\omega = 0.1$ in different temperatures: (a) swollen state at $T^* = 1.2$, (b) coil-to-globule transition at $T^*_{CG} = 0.85$, (c) four-cluster structure at $T^* = 0.75$, (d) tricluster structure at $T^* = 0.62$, and (e) dicluster structure at $T^* = 0.5$.

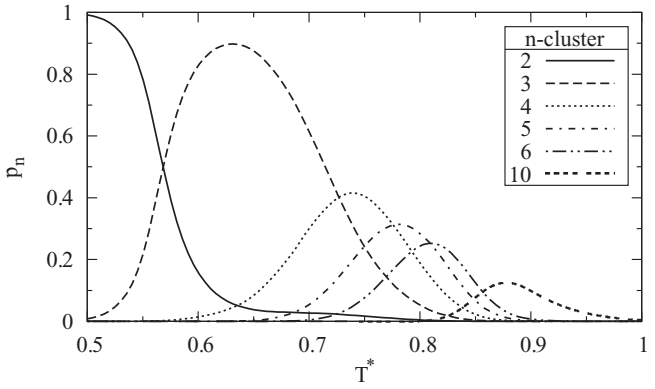

FIG. 3. Probability of finding the n-cluster structure p_n as a function of reduced temperature T^* for the $(10\text{-}10)_{12}$ chain with compatibility $\omega = 0.1$. For clarity, only selected p_n lines are shown.

This effect can be quantified by a CCD diagram for different T^* as shown in Fig. 3. As the system is cooled down to a globular state, the nanostructures with less clusters are more likely to be formed.

For $T^* \approx T^*_{CG}$, about seven to ten clusters are the most probable. The corresponding structures are loosely packed disordered globules as shown in in Fig. 2(b). At $T^* = 0.75$, the most probable structure is a four cluster [Fig. 2(c)] with a probability of about 0.4, however, a tricluster [Fig. 2(d)] and a five cluster are also very likely to be seen with probabilities of about 0.3 and 0.25, respectively. The remaining probability 0.05 is distributed for the six-cluster and dicluster structures. Then, for $T^* = 0.62$, we observe a maximum in CCD for tricluster structures with a probability of 0.9. This seems to correspond to the minimum in C_v for this T^*. Finally, at $T^* = 0.56$, we see that tricluster and dicluster [Fig. 2(e)] structures are equally probable with a probability of 0.5 (it corresponds to the second peak in C_v). At lower T^*, we observe dicluster structures with a probability approaching 1.

As noted above, for $T^* = 0.56$, we observe both a maximum in C_v and a transition from tricluster to dicluster structures in the CCD diagram. From this observation, we suggest that the C_v bump for $T^* \approx 0.75$ is caused by structural changes from six cluster, through five and four cluster, to a tricluster in this region.

Next, we simulate multiblocks with gradually higher compatibility parameters, from $\omega = 0.2$ to 1.0. We show only representative CCD diagrams (Fig. 4). As we increase ω, the coil-to-globule transition occurs at gradually higher T^*'s. In Fig. 5, we show this transition for different ω's, and as it is increased, transformations between intraglobular structures with different numbers of clusters shift to higher T^*'s in accordance with the T^*_{CG}'s behavior.

In Fig. 4(a), we show the CCD for $\omega = 0.6$. For T^*'s between 0.6 and 0.7, the probability of finding dicluster structures increases noticeably (compare with Fig. 3) and reaches about 0.3. For $\omega = 0.7$ [Fig. 4(b)] and the same T^* range, the probabilities of finding diclusters and triclusters are almost equal. Further increasing in ω [Figs. 4(c) and 4(d)] causes a higher probability of finding diclusters in this region with probabilities of about 0.6 and 0.9 for $\omega = 0.8$ and 1.0, respectively.

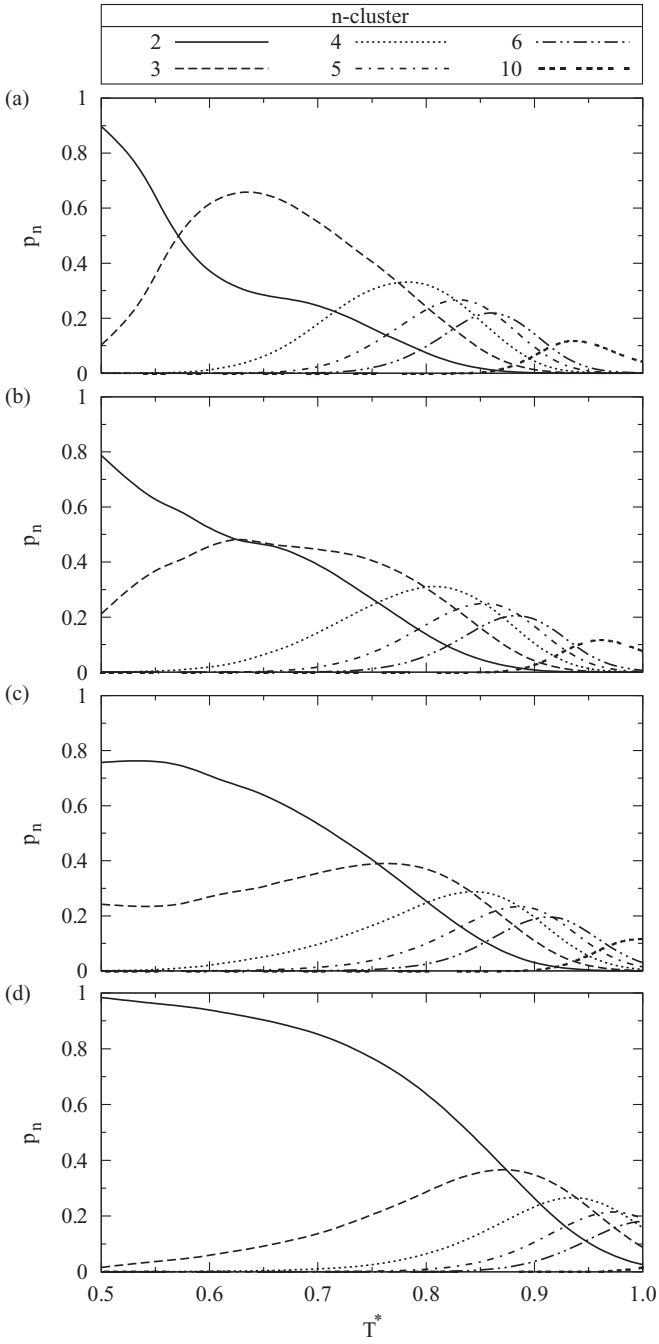

FIG. 4. Probability of finding the n-cluster structure p_n as a function of reduced temperature T^* for the $(10\text{-}10)_{12}$ chain with compatibility: (a) $\omega = 0.6$, (b) $\omega = 0.7$, (c) $\omega = 0.8$, and (d) $\omega = 1.0$. For clarity, only selected p_n lines are shown.

This effect can be interpreted in terms of the site percolation problem [31]. For the highest compatibility $\omega = 1$, A and B monomers can freely mix, since energetically, they are indistinguishable. In this case, the copolymer chain becomes a homopolymer, and the clusters have no physical meaning, but we analyze them formally in order to be consistent with the rest of this paper. The effect described in this paragraph is also relevant to other ω's, but for lower ω's, monomers are less miscible. At low T^*'s, the monomers are densely packed spheres in a globule, and most of them have $Z = 12$ nearest

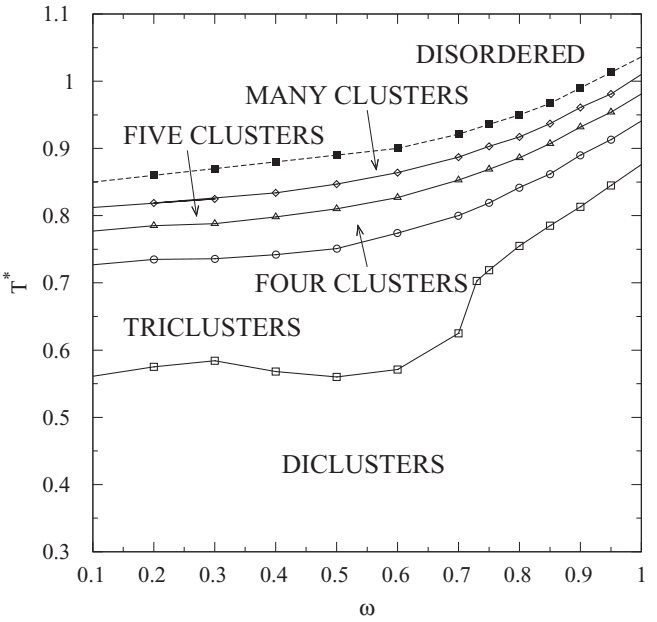

FIG. 5. Phase diagram for the $(10\text{-}10)_{12}$ chain in (T^*,ω) space. The dashed line shows coil-globule transition. The solid lines divide regions with the greatest probability of finding n-cluster structures. The many-cluster region consists of structures with $n > 5$ clusters.

neighbors. Since the type of two neighboring monomers is fixed (these are monomers along the chain—with an exception of the terminal monomers, which only have one type of fixed neighbor), only $Z = 10$ neighbors are of varied types. Critical percolation threshold for a face centered cubic lattice (which can be used here since we have densely packed spheres in a globule) is $p_c \approx 0.119$ [31]. In our case, since we have 120 A and 120 B monomers, $p \approx 0.5$. Moreover, in the case of the $(10\text{-}10)_{12}$ chain, there are always blocks of ten monomers of the same type, therefore, in this case, it is sufficient that only one of ten monomers from the block has contact with another monomer of the same type in order to observe the percolation effect. Therefore, the dicluster structures (in which each monomer type creates a continuous phase within a globule) are very common.

For a better insight into dicluster structures, we show representative snapshots of these structures at $T^* = 0.5$ (Fig. 6). As we increase ω from 0.1 to 0.5, the structural changes are small [compare Fig. 2(e) with Fig. 6(a)], then, as we increase it further, handshake structures prevail. In Fig. 6(b), we show a handshake structure and, in Fig. 6(c), the same structure without B monomers. For $\omega = 0.9$, we find many handshake structures and tori with a core, where one type of monomer forms a torus around the other type [Fig. 6(d)]. Then, for $\omega = 0.95$, we find more disordered structures, but very often, monomers of the same type seem to aggregate [Fig. 6(e)]. Finally, for $\omega = 1$, we observe disordered dicluster globules.

In Fig. 5, we show a phase diagram that collects data from all ω's for the $(10\text{-}10)_{12}$ chain. We want to stress that intraglobular structure is not exclusively defined by the number of clusters and that the presented phase diagram shows regions with the most probable structures but others are also present with smaller probabilities.

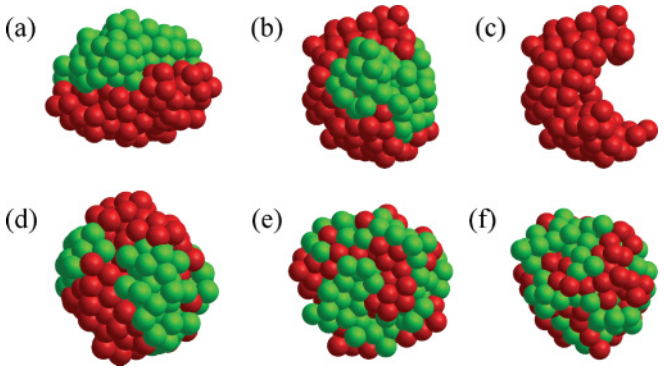

FIG. 6. (Color online) Variety of dicluster structures for the $(10\text{-}10)_{12}$ chain at $T^* = 0.5$ for compatibility: (a) $\omega = 0.5$, (b) $\omega = 0.8$, (c) $\omega = 0.8$ (without B monomers), (d) $\omega = 0.9$, (e) $\omega = 0.95$, and (f) $\omega = 1$.

B. Structure factor

Since the CCD for a globule is not easily measurable experimentally, we calculate the structure factor (measured in scattering experiments) $S(k)$ for the smallest compatibility $\omega = 0.1$. We select A monomers as the scattering centers and calculate the isotropic $S(k)$ as follows:

$$S(k) = \frac{1}{N}\sum_{n,m}\frac{\sin\, kr_{nm}}{kr_{nm}}, \tag{6}$$

where k is a scattering vector length and r_{nm} is a distance between monomer n and m. Results are presented in Fig. 7.

For all T^*'s, we can observe a small maximum at $k \approx 0.94$, which corresponds to a length of about 6.7σ. Since it is also visible for T^*'s above T^*_{CG}, we can conclude that it corresponds to the extended size of a single block, which is 10σ.

For $T^* = 0.7$ and 0.6, we can see another small maximum for $k \approx 1.7$, which corresponds to length 3.7σ. As we observe in Fig. 5, the most probable structure for those T^*'s is a tricluster for which the thickness of the middle cluster of the globule is about 4σ. Therefore, we think that this maximum is related to layers in the tricluster structures. This maximum

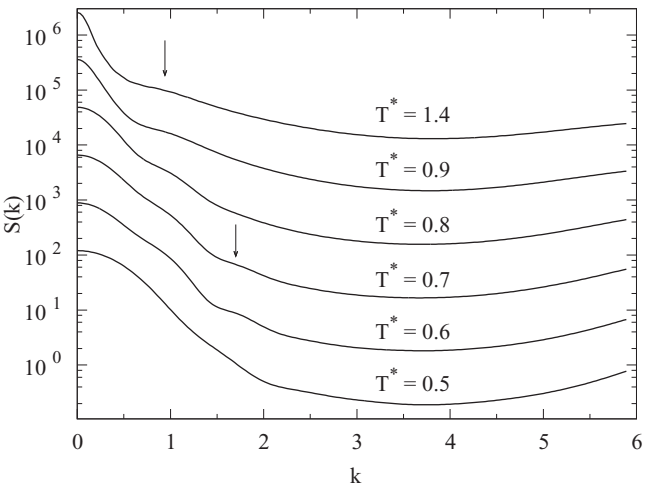

FIG. 7. Structure factor $S(k)$ for the $(10\text{-}10)_{12}$ chain with $\omega = 0.1$ at $T^* = 1.4$, 0.9, 0.8, 0.7, 0.6, and 0.5. The scattering profiles are offset vertically by factors of 10, 10^2, 10^3, 10^4, and 10^5, for clarity.

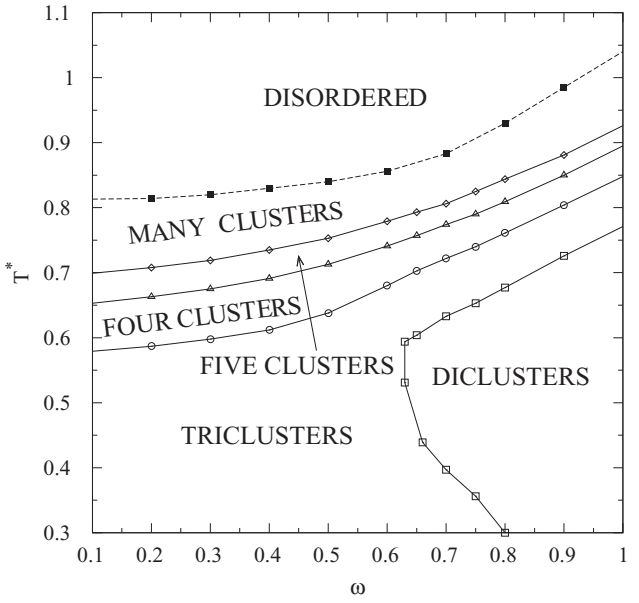

FIG. 8. Phase diagram for the $(6\text{-}6)_{20}$ chain in (T^*,ω) space. The dashed line shows coil-globule transition. The solid lines divide regions with the greatest probability of finding n-cluster structures. The many-cluster region consists of structures with $n > 5$ clusters.

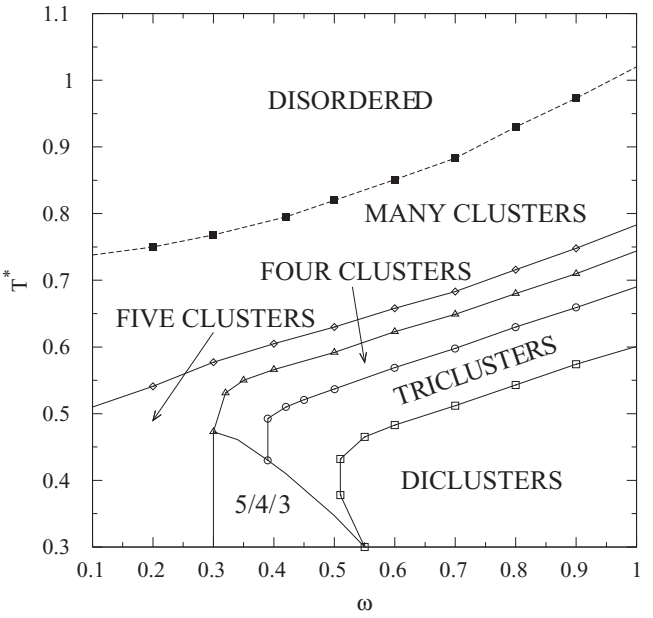

FIG. 9. Phase diagram for the $(3\text{-}3)_{40}$ chain in (T^*,ω) space. The dashed line shows coil-globule transition. The solid lines divide regions with the greatest probability of finding n-cluster structures. The many-cluster region consists of structures with $n > 5$ clusters. In the $5/4/3$ region, the probabilities of finding five, four, and triclusters is almost equal.

is not visible for $T^* = 0.5$. At this temperature, the most probable structure is a dicluster and, since we scatter on A monomers, we should obtain the structure factor of a flattened globule.

The above results indicate that the tricluster and dicluster structures may be distinguished experimentally by the $S(k)$ measurements.

C. Cluster count diagrams for other chain microarchitectures

The same procedure, as described above, is performed for $(6\text{-}6)_{20}$ and $(3\text{-}3)_{40}$ chains, and the results are presented in Figs. 8 and 9. In the case of these chain microarchitectures, it is necessary to simulate them at lower T^*'s than those for the $(10\text{-}10)_{12}$ chain, because many structural changes occur at lower temperatures.

First, we discuss results for the $(6\text{-}6)_{20}$ chain. The coil-to-globule transition occurs at a lower temperature because the energy variations are smaller than those for the $(10\text{-}10)_{12}$ chain. This is related to a higher number of A-B contacts along the chain and the fact that those contacts do not contribute effectively to the interaction energy.

In general, the regions of dominance for the four clusters and n clusters (with $n > 4$) is similar to that for the $(10\text{-}10)_{12}$ chain, but it is different for di- and triclusters. We can see that tricluster structures for $\omega < 0.6$ are the most probable at low temperatures, whereas, for the previously discussed chain, the dicluster structures prevail. This effect is explained in the next section in terms of the interfacial surface minimization.

For $\omega > 0.6$, we observe a behavior similar to that of the $(10\text{-}10)_{12}$ chain. Monomers of different types mix and finally form a disordered dicluster within globules, as explained earlier in terms of the site percolation problem.

Figure 10 presents selected snapshots of structures observed for this chain. In Fig. 10(a), we see a tricluster for $\omega = 0.1$ with flat A-B interfaces. This structure dominates over a wide range of ω's. However, as we increase ω's, those tricluster

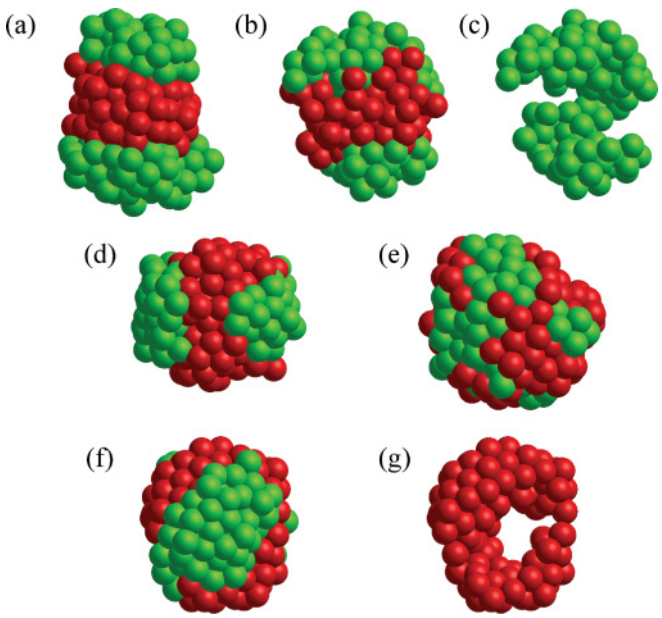

FIG. 10. (Color online) Variety of structures for the $(6\text{-}6)_{20}$ chain at $T^* = 0.3$ for compatibility: (a) $\omega = 0.1$ (tricluster), (b) $\omega = 0.7$ (at $T^* = 0.5$, dicluster), (c) $\omega = 0.7$ (at $T^* = 0.5$, without B monomers, dicluster), (d) $\omega = 0.7$ (tricluster), (e) $\omega = 0.9$ (dicluster), (f) $\omega = 0.8$ (dicluster), and (g) $\omega = 0.8$ (without B monomers, dicluster).

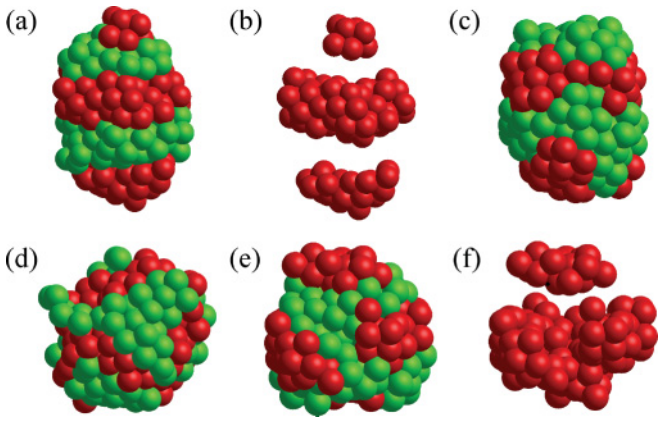

FIG. 11. (Color online) Variety of structures for the $(3\text{-}3)_{40}$ chain at $T^* = 0.3$ for compatibility: (a) $\omega = 0.1$ (five cluster, lamellar), (b) $\omega = 0.1$ (without B monomers, five cluster, lamellar), (c) $\omega = 0.31$ (four cluster, lamellar), (d) $\omega = 0.5$ (at $T^* = 0.5$, tricluster), (e) $\omega = 0.51$ (tricluster), and (f) $\omega = 0.51$ (without B monomers, tricluster).

structures become more spherical, for example, see Fig. 10(d) for $\omega = 0.7$, where the interfaces between A and B phases are more curved (such as in handshake structures). For the same ω, but at higher T^*'s, dicluster structures dominate, exhibiting handshake structures, spiral structures [Figs. 10(b) and 10(c)], and others.

For $\omega \geqslant 0.8$, dicluster structures prevail in a wider T^* range. Those dicluster structures are very similar to those mentioned in the previous paragraph. Also, a torus with a core appears here [Figs. 10(f) and 10(g)].

Finally, the $(3\text{-}3)_{40}$ microarchitecture is considered. The coil-to-globule transition occurs in lower T^*'s (Fig. 9) because there are more contacts between A and B monomers along the chain and, therefore, lower total energy.

Structures with a specified number of clusters occur in the same order as for the other chain architectures, but they appear at lower T^*'s. For $\omega \leqslant 0.3$, the most probable structures consist of five clusters arranged in layers [Figs. 11(a) and 11(b)]. For $\omega > 0.3$ at $T^* \approx 0.5$, we find four-cluster structures, and in lower T^*, there is a region where five, four, and tricluster structures were almost equally probable and, in our simulations, we could not identify the dominating one. For $\omega > 0.4$, the tricluster structures dominate, and for $\omega > 0.52$, dicluster structures dominate at low T^*'s. Again, those dicluster structures are mixed A and B monomers, and they appear for similar parameters (high ω and low T^*) as for the previously discussed chains.

Figure 11 presents snapshots of selected structures for the $(3\text{-}3)_{40}$ chain. We notice that increasing ω yields more curved structures, for example, the globule in Fig. 11(a) has a rather flat interface between A and B phases, but in Fig. 11(c), those interfaces are more curved. As they become more curved, they tend to connect with other layers [see Figs. 11(d)–11(f)].

D. Types of observed structures

Structural changes observed in this paper can be considered a result of the competition between two effects: minimization of the A-B interfacial area, that is, the number of contacts between A and B, and the minimization of the interfacial area between the chain and the solvent, that is, the number of contacts between the chain and the solvent. Those effects are additionally influenced by the chain microarchitecture.

If we consider a mixture of spheres of two incompatible types, we will observe formation of two separate A- and B-rich phases. Adding bonds between spheres frustrates the phase separation, and this system tries to find a structure, satisfying the chain microarchitecture constraints, with the minimum number of A-B contacts. For example, in symmetric diblock copolymer melts, one can observe lamellar structures with flat A-B interfaces [3]. Asymmetric diblock melts [32] or symmetric diblock melts with a solvent [3] form other nonlamellar structures, such as gyroid, cylinders, and spheres.

On the other hand, in dilute polymer solutions, another minimization effect is also significant. Chains in a bad solvent minimize their contacts with the solvent and form spherical globules because the sphere has the minimum surface area for a given volume. For block copolymer melts, a spherical confinement can be introduced artificially. As shown in Refs. [8,9], this confinement can yield structures similar to those presented in this paper.

We assume, for the sake of this discussion, that the entropic effects are less significant and are not addressed. The observed structures are thought to be a result of a delicate interplay between the two above enthalpic effects. Varying ω's changes the relative contributions of those two effects. Increasing ω makes the first effect less significant. In the limit $\omega = 1$, the first effect disappears (since A and B monomers are fully miscible). From snapshots presented in this paper, it can be seen that, for chains with higher ω's, globules are more spherical than those with lower ω's.

As an example, we consider the formation of tricluster structures in the $(6\text{-}6)_{20}$ chain for $\omega = 0.1$ at $T^* < 0.58$. Figure 10(a) presents a snapshot of a globule for those parameters. It is a tricluster structure with clusters arranged in layers with almost flat A-B interfaces. This globule has an elliptical shape. Diclusters with a flat A-B interface seem to provide the smallest possible interfacial area, but to keep it flat, a globule as a whole must be considerably flattened, which increases the contacts between chain and solvent. On the other hand, compacting it into a more spherical shape increases the A-B interface curvature. As a result, one type of monomer forms two separate clusters, which order lamellarly. Increasing ω results in forming more spherical globules and, therefore, in increasing interface area between different types of monomers (see Fig. 10), since, as described earlier, the A-B penalty for contacts is smaller for higher ω's.

Within-globular orderings can be related to the nanophase separations in block copolymers because a globule is a locally dense system. Since only symmetric block sizes were used in this paper, structures should correspond to bulk symmetric diblock copolymers. In such systems, lamellar phases are expected (however, gyroid, perforated lamellae, cylinders, and other structures were recently found in sulfonated diblock copolymers with symmetric block sizes both in experiment [33] and in simulation [34]). Changing the A-B interaction potentials should only shift the order-disorder transition temperature, and it should not easily lead to the formation

of nonlamellar structures. Why, therefore, do we observe handshake, spiral, and other nonlamellar configurations? As indicated earlier, we consider it a result of a delicate interplay of two effects. As we increase compatibility, the minimization of contacts between chain and solvent becomes a stronger effect than the minimization of the A-B interfacial area, and in order to form more spherical shapes of a globule, the A-B interfaces tend to be more curved. Thus, as a result, we obtain the handshake, the spiral, and other structures.

We conjecture that asymmetric block sizes are necessary to obtain gyroidlike structures within a single globule. However, they were not considered in this paper. Probing different microarchitectures may lead to many other structures, for example, sufficiently long chains should reproduce a richer phase diagram with cylindrical, gyroidal, or spherical intraglobular structures.

E. Intraglobular structures and native states of proteins

This coarse-grained model is probably too simplified to capture the complexity of protein behavior, but it still may shed some light on it. For example, in order to create helical structures, hydrogen bonds are necessary [13]. Therefore, the spiral structures observed in this paper are not a manifestation of the helical-like structures found in polypeptide chains because our spirals are relatively thick—on the order of few monomers in diameter [see Fig. 10(c)].

Amino acids can be divided roughly into two groups: H and P. Most of the simplified coarse-grained protein models mainly capture this property. However, in our model, the solvent is nonselective, and it becomes poor when we decrease T^*. Therefore, we can consider those globules as H cores consisting of two types of amino acids.

In this paper, we do not observe a single native state. As can be seen in CCD diagrams (Figs. 3 and 4) for a given T^*, structures with different numbers of clusters can coexist. Only for the lowest T^*'s does the probability of finding structures with a given number of clusters approach 1. But even in such a case, there is degeneration of native states because in order to obtain it, a chain can be folded in a variety of ways. For example, in order to form a dicluster structure, such as in Fig. 6(a), it does not matter where different A blocks are, as long as they are inside the A cluster.

However, we would like to emphasize that the low compatibility between monomers reduces the degeneracy of the interglobular structures. There are less possible ways to fold a chain into a lamellarlike structure than into a disordered globule.

V. CONCLUSION

We present an extensive MC study of intraglobular structures of long multiblock copolymer chains with alternating blocks, using a discontinuous interaction potential.

Due to the chain architecture constraints, the interplay of minimization of the A-B interface with the minimization of the polymer-solvent interface yields a rich phase diagram with a variety of intraglobular structures, such as handshake, spiral, tricluster, torus with a core, lamellar, and many other mixed and disordered structures. We relate our results to those for block copolymer nanophases in bulk and find many similarities between them, especially in spherical confinement. We also expect that other intraglobular structures may be present in multiblock copolymer chains with asymmetric blocks, such as analogs of gyroidal, cylindrical, and spherical nanophases.

We analyzed the $(10\text{-}10)_{12}$ chain behavior for various T^*'s and ω's. From this analysis and similar analyses of other chains [$(6\text{-}6)_{20}$ and $(10\text{-}10)_{12}$], we construct phase diagrams in the (T^*,ω) space of the most probable n-cluster structures. In each case, decreasing T^* leads to coil-to-globule transition, followed by transitions between structures with n clusters (n decreases with T^*). The smallest n for low ω and low T^* was 2, 3, and 5 for $(10\text{-}10)_{12}$, $(6\text{-}6)_{20}$, and $(3\text{-}3)_{40}$, respectively.

From the structure factor of the $(10\text{-}10)_{12}$ chain, we can distinguish tricluster and dicluster structures, and, therefore, it is possible to relate the numerical predictions to an experiment.

Finally, we show that, despite the simplicity of this model, it still may shed some light on the highly complex behavior of proteins, for example, varying compatibility between monomers within H cores may reduce the degeneracy of the ground states.

ACKNOWLEDGMENTS

We gratefully acknowledge the computational grant from the Poznan Supercomputing and Networking Center (PCSS) and Grant No. N202 287338 from the Polish Ministry of Science and Higher Education.

[1] D. F. Parsons and D. R. M. Williams, Phys. Rev. Lett. **99**, 228302 (2007).
[2] I. W. Hamley, *Developments in Block Copolymer Science and Technology* (Wiley, Berlin, 2004).
[3] S. Woloszczuk, M. Banaszak, P. Knychala, and M. Radosz, Macromolecules **41**, 5945 (2008).
[4] P. Cheolmin, Y. Jongseung, and L. T. Edwin, Polymer **44**, 6725 (2003).
[5] W. Li, R. A. Wickham, and R. A. Garbary, Macromolecules **39**, 806 (2006).
[6] X. He, M. Song, H. Liang, and C. Pan, J. Chem. Phys. **114**, 10510 (2001).
[7] B. Yu, P. Sun, T. Chen, Q. Jin, D. Ding, B. Li, and A. Shi, J. Chem. Phys. **126**, 204903 (2007).
[8] B. Yu, B. Li, Q. Jin, D. Ding, and A. Shi, Macromolecules **40**, 9133 (2007).
[9] S. Piotto, S. Concilio, F. Mavelli, and P. Iannelli, Macromol. Symp. **286**, 25 (2009).
[10] S. Schnabel, M. Bachmann, and W. Janke, J. Chem. Phys. **131**, 124904 (2009).
[11] S. Schnabel, T. Vogel, M. Bachmann, and W. Janke, Chem. Phys. Lett. **476**, 201 (2009).
[12] D. T. Seaton, T. Wüst, and D. P. Landau, Phys. Rev. E **81**, 011802 (2010).

[13] E. Shakhnovich, Chem. Rev. **106**, 1559 (2006).
[14] Y. S. Djikaev and E. Ruckenstein, Adv. Colloid Interface **146**, 18 (2009).
[15] J. Schluttig, M. Bachmann, and W. Janke, J. Comput. Chem. **29**, 2603 (2008).
[16] J. N. Onuchic, P. G. Wolynes, Z. Luthey-Schulten, and N. D. Socci, Proc. Natl. Acad. Sci. USA **92**, 3626 (1995).
[17] K. Yue, K. M. Fiebig, P. D. Thomas, H. S. Chan, E. I. Shakhnovich, and K. A. Dill, Proc. Natl. Acad. Sci. USA **92**, 325 (1995).
[18] R. Schiemann, M. Bachmann, and W. Janke, J. Chem. Phys. **122**, 114705 (2005).
[19] J. Straub and D. Thirumalai, Proc. Nad. Acad. Sci. USA **90**, 809 (1993).
[20] S. Miyazawa and R. L. Jernigan, J. Mol. Biol. **256**, 623 (1996).
[21] E. I. Shakhnovich, Phys. Rev. Lett. **72**, 3907 (1994).
[22] Y. Zhou, C. K. Hall, and M. Karplus, Phys. Rev. Lett. **77**, 2822 (1996).
[23] K. Lewandowski, P. Knychala, and M. Banaszak, Phys. Status Solidi B **245**, 2524 (2008).
[24] S. Woloszczuk, M. Banaszak, P. Knychala, K. Lewandowski, and M. Radosz, J. Non-Cryst. Solids **354**, 4138 (2008).
[25] K. Lewandowski and M. Banaszak, J. Non-Cryst. Solids **355**, 1289 (2009).
[26] N. Metropolis, A. Rosenbluth, M. Rosenbluth, and A. Teller, J. Chem. Phys. **21**, 1087 (1953).
[27] D. J. Earl and M. W. Deem, Phys. Chem. Chem. Phys. **7**, 3910 (2005).
[28] H. G. Katzgraber, S. Trebst, D. A. Huse, and M. Troyer, J. Stat. Mech. P03018 (2006).
[29] K. Lewandowski, P. Knychala, and M. Banaszak, Comput. Methods Sci. Technol. **16**, 29 (2010).
[30] T. Beardsley and M. Matsen, Eur. Phys. J. E **32**, 255 (2010).
[31] M. Sykes, D. Gaunt, and M. Glen, J. Phys. A **9**, 1705 (1976).
[32] M. Matsen, G. Griffiths, R. Wickham, and O. Vassiliew, J. Chem. Phys. **124**, 024904 (2006).
[33] M. J. Park and N. P. Balsara, Macromolecules **41**, 3678 (2008).
[34] P. Knychala, M. Banaszak, M. J. Park, and N. P. Balsara, Macromolecules **42**, 8925 (2009).